RSC Advances

ROYAL SOCIETY OF CHEMISTRY

www.rsc.org/advances

Table of contents entry

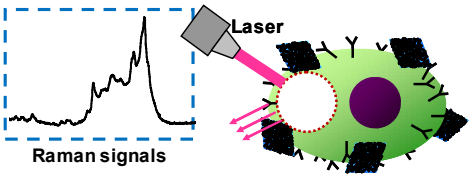

SERS Probe for Cancer Diagnostics

A SERS-active detection platform based on the ultrathin g-C_3N_4 nanosheets/Au@AgNPs hybrids (g-C3N4/Au@AgNPs) was developed for ultrasensitive Raman signal readout and Cancer Cells Diagnostics.

Cite this: DOI: 10.1039/c0xx00000x

COMMUNICATION

www.rsc.org/ advances

Synthesis of g-C_3N_4 Nanosheets/Au@Ag Nanoparticles Hybrids as SERS Probe for Cancer Cells Diagnostics

Jianping Wang,[a,b] Renyong Liu,[a] Cheng Zhang,[a,b] Guangmei Han,[a] Jun Zhao,[a] Bianhua Liu,*[,a] Changlong Jiang*[,a] and Zhongping Zhang[a,c]

Received (in XXX, XXX) Xth XXXXXXXXX 20XX, Accepted Xth XXXXXXXXX 20XX
DOI: 10.1039/b000000x

The chemical sensing for the convenient diagnosis of cancer cells has been widely exploed with the use of various sensing materials and techniques, but it is still a challenge to achieve ultrasensitive, simple, rapid and inexpensive detection for cancer cells. Herein, we report a surface-enhanced Raman scattering (SERS) method for the detection of cancer cells in *situ*. In our work, the ultrathin g-C_3N_4 nanosheets/Au@AgNPs hybrids (g-C_3N_4/Au@AgNPs) were fabricated by self-assembly strategy, in which poly (ethyleneimine) (PEI) was used to obtain cationic polyelectrolyte modified ultrathin nanosheets and anchor the Au@AgNPs. The g-C_3N_4 nanosheets exhibited strong enrichment ability and the self-assembled Au@AgNPs showed excellent SERS activity, both of which led to an ultrahigh sensitivity. The hybrids were applied to detect folic acid (FA) with the sensitive limit of 2.41 nM. Importantly, after being modified with FA which targeted cancer cells with folate receptors (FRs), the formed g-C_3N_4/Au@AgNPs-FA was used as SERS probe for the on-site monitoring of cancer cells with FA as Raman reporter molecules.

1. Introduction

SERS has been widely used as a very important analytical technique with impressive sensitivity in a number of applications, such as food safety,[1] explosives detection,[2] environmental monitoring,[3] biomedical research,[4] bioimaging[5] and so on. Noble metal nanoparticles (Au, Ag) are often chosen for fabricating SERS substrates because of their optical activity by supporting localized surface plasmon resonances (LSPRs).[6] SERS could provide the signal intensity of the molecules that on or near the substrates by orders of magnitude, even with the ability of single molecules detection.[7] Compared to individual nanoparticles, the Ag/Au-based composite materials have gradually attracted attentions for well-defined structures, higher Raman activity, better stability and biocompatibility.[8] However, it is still a challenge to fabricate the SERS substrates with large enhancement ability and good reproducibility, particularly for these molecules which have poor affinity to the noble metals.

In the past few years, the ultrathin two-dimensional (2D) layered nanomaterials have attracted tremendous attention from people for their excellent electronic, optical, biological compatibility, and high surface areas in contrast to the bulk materials.[9] As an analogue of graphite, graphitic-phase carbon nitride (g-C_3N_4) is the most stable allotrope of carbon nitride.[10] The ultrathin g-C_3N_4 nanosheets have high surface-to-volume ratio, good biocompatibility and low toxicity, which shows great potential applications in Cu^{2+} detection,[11] glucose detection,[12] drug delivery[13]and bioimaging.[14] Furthermore, the ultrathin g-C_3N_4 nanosheets are considered as a prospective supporting material for metal nanoparticles to form hybrids. Here, a self-assembly strategy was developed to obtained g-C_3N_4/Au@AgNPs hybrids, in which PEI was used to functionalize g-C_3N_4 nanosheets and anchor the Au@AgNPs.[15] The above hybrids could be used as SERS-active material, in which Au@AgNPs could enhance Raman scattering while g-C_3N_4 could concentrate the molecules with high enrichment capacity. The hybrids were used as the SERS substrate to detect R6G with an enhancement factor as high as 3.0×10^{16}. Moreover, the as-fabricated substrate could be apply to enhance the Raman signals of folic acid (FA), showing a detection limit as low as 2.41 nM.

FA is a typical cell-targeting agent, which has high affinity with folate receptors (FRs). The FRs are overexpressed on the surface of some human cancer cells and are absent on normal cells, as a result, the FR could be used to distinguish the cancer and normal cells.[16] Up to now, FA-containing nanomaterials have been developed to target cancer cells owing to the FA has very high affinity to the FRs on the cancer cells. Taking into account of fluorescence based techniques exhibited some disadvantages such as spectral overlap, the SERS had extremely high sensitivity and sharp peaks which can be used to distinguish multiple analytes in a mixture. The modification of FA on the nanomaterials mainly in two ways: covalent[17]and noncovalent[18] binding. In contrast to covalent modification, the noncovalent

binding has less impact on the materials. With such effect, the modification of FA by physisorption may provide a reliable, simple and highly efficient way.

In this paper, a facile and efficient SERS probe was prepared and used for cancer diagnosis, which was composed of g-C_3N_4/Au@AgNPs hybrids and FA (g-C_3N_4/Au@AgNPs-FA). The above-mentioned SERS probe was used to detect the cancer cells, and exhibited very low toxicity. It was mentioned that the FA were used as both Raman reporter molecule and the targeting ligand with the cancer cells. Finally, the excellent SERS and cell targeting properties of g-C_3N_4/Au@AgNPs-FA were investigated by HeLa cells which over-express the FRs (FRs-positive) and A549 cells as control which express few FRs (FRs-negative).

2. Experimental section

2.1 Materials

Sodium citrate ($Na_3C_6H_5O_7 \cdot 2H_2O$, 99.8%), silver nitrate ($AgNO_3$, 99%), chloroauric acid ($HAuCl_4 \cdot 4H_2O$, 99.9%), polyvinyl pyrrolidone (PVP), melamine were purchased from Sinopharm Chemical Reagent Co., Ltd. (Shanghai, China). Poly(ethyleneimine) (PEI), folic acid (FA) and 3-(4,5-dimethyl thiazol-2-yl)-2,5-diphenyltetrazolium bromide (MTT) were purchased from Sigma-Aldrich. All of these chemical regents were used without further purification. Ultrapure water (18.2 MΩ•cm) used in all reactions was produced by Millipore water purification system.

2.2 Synthesis of Au@Ag nanoparticles

The AuNPs were used as seeds to prepare Au@Ag nanoparticles. Firstly, the AuNPs were obtained by the reduction of $HAuCl_4$ with sodium citrate. Typically, 1.5 mL of 1% trisodium citrate was quickly injected into boiling ultrapure water (100 mL) which contained 2.5×10^{-5} M $HAuCl_4$. Then, the mixture was kept boiling for 30 min. At last, the solution became wine red and Au NPs were synthesized. Secondly, 4 mL of 1% trisodium citrate was added into the Au NPs solution. Then 1 mM $AgNO_3$ (17 mL) was added drop by drop into the above mixture. The $AgNO_3$ could be reduced on the surface of the AuNPs to form Au@AgNPs. At last, the color of the solution changed from wine red to orange yellow.

2.3 Synthesis of Ag nanoparticles

The AgNPs were synthesized by the reduction of $AgNO_3$ with sodium citrate. In detail, the 250 mL of aqueous solution containing 90 mg $AgNO_3$ was first heated to boil, then 1% sodium citrate (10 mL) was quickly injected into the above boiling solution. After refluxing for 1 h, the resultant yellow-green colloid was cooled to room temperature.

2.4 Synthesis of bulk g-C_3N_4

The bulk g-C_3N_4 was obtained by the polymerization of melamine molecules at 600 ^oC under air condition, and then kept at that temperature for 2 h.[14] The melamine was heated to 600 ^oC with a constant heating rate of 3 ^oC min^{-1}, and the same ramp rate was controlled for the cooling process.

2.5 Synthesis of ultrathin g-C_3N_4 nanosheets

The ultrathin g-C_3N_4 nanosheets were prepared by ultrasound of as-prepared bulk g-C_3N_4 in water for about 20 h.[14] Subsequently, the formed suspension was centrifuged at 6000 rmp to eliminate the unexfoliated g-C_3N_4 before further used.

2.6 Synthesis of PEI-functionalized ultrathin g-C_3N_4 nanosheets

In a typical procedure, 60 mg of PVP was added to 100 mL ultrathin g-C_3N_4 nanosheets solution, followed by ultrasound for 30 min and stirring for 90 min. The obtained solution was washed two times at 6000 rmp for 20 min to remove the free PVP, and then dispersed into 10 mL ultrapure water. To obtain PEI-functionalized ultrathin g-C_3N_4 nanosheets, 7 mL of 1% PEI was mixed well with 40 mL of 0.5 M KCl, then the above PVP-capped ultrathin g-C_3N_4 nanosheets was added. The final solution was sonicated for 90 min. The obtained solution was washed three times at 6000 rmp for 8 min to remove the free PEI, and then the synthesized PEI/ultrathin g-C_3N_4 nanosheets was redispersed in 10 mL ultrapure water.

2.7 Synthesis of ultrathin g-C_3N_4 nanosheets/Au@Ag nanoparticles hybrids (g-C_3N_4/Au@AgNPs)

500 μL of PEI/ultrathin g-C_3N_4 nanosheets was added into 5 mL Au@Ag nanoparticles solution under ultrasound before placed overnight. Finally, the obtained g-C_3N_4/Au@AgNPs hybrids was washed three times with ultrapure water and redispersed. The ultrathin g-C_3N_4 nanosheets/AgNPs (g-C_3N_4/AgNPs) nanocomposites was also obtained similarly.

2.8 Synthesis of ultrathin g-C_3N_4 nanosheets/Au@Ag nanoparticles-FA (g-C_3N_4/Au@AgNPs-FA)

The loading of FA on ultrathin g-C_3N_4 nanosheets/ Au@Ag was obtained by mixing g-C_3N_4/Au@AgNPs with FA (1×10^{-4} M) solution overnight. After that, the unbound FA was washed by centrifugal washing. At last, the g-C_3N_4/Au@AgNPs-FA was redispersed into PBS buffer (pH~7.4) for further use.

2.9 Cell culture and viability measurements

The HeLa cells and A549 cells were cultured in high glucose Dulbecco's modified Eagle's medium (DMEM, Invitrogen, Carlsbad, CA), which supplemented with 10% (v/v) fetal bovine serum (FBS, Invitrogen), penicillin (100 units/mL), and streptomycin (100 g/mL) at 37 ^oC in a humidified incubator (MCO-18AC, Sanyo, Japan) containing 5% CO_2. The effect of g-C_3N_4/Au@AgNPs-FA on cell proliferation was investigated by MTT assay. Firstly, the HeLa cells were seeded onto the 96-well plate and incubated for 24 h. After that, g-C_3N_4/Au@AgNPs-FA with predetermined concentration (0, 75, 150, 300, 450 μg/mL) was added to the cells. After 24 h incubtation, the medium was changed to MTT solution, and the cells were incubated for another 4 h. Finally, the Bio-Rad ELISA reader was used to measure the viability of cells at 570 nm. As contrast, cells were incubated in the absence of g-C_3N_4/Au@AgNPs-FA.

2.10 SERS detection of live cancer cells

The HeLa cells and A549 cells were seeded into the sterile glass coverslips culture petri dishes and incubated for 24 h. Then, the culture medium was changed to the culture medium containing g-C_3N_4/Au@AgNPs-FA and incubated for another 2 h at 37 ^oC. Before measurement, the culture dishes were washed three times

to remove the free g-C_3N_4/Au@AgNPs-FA. The Raman measurements were performed using a 532 nm laser and 10× objective, laser power 2 mW, and the acquisition time 2 s, respectively. The Raman Mapping for cell was carried out by DXR Raman microscopy with 532 nm laser (2 mW) and 50× objective lens, the accumulation time for each spectrum was 1 s.

2.11 Measurements

The UV-vis absorption spectra were recorded with a Shimadzu UV-2550 spectrometer. The ultrathin g-C_3N_4 nanosheets and Au@AgNP$_S$ were characterized by transmission electron microscopy (TEM, JEOL-2010) and field-emission scanning microscopy (FE-SEM, Sirion-200). Atomic force microscopy (AFM) images were obtained on a DI Innova. The Zeta-potential measurements was measured using a Zetasizer 3000 HSA. Raman measurements were conducted with Thermo Fisher DXR Raman Microscope equipped with a CCD detector with the excitation wavelength of 532 nm. The XRD was recorded on a MAC Science Co. Ltd. MXP 18 AHF X-ray diffractometer.

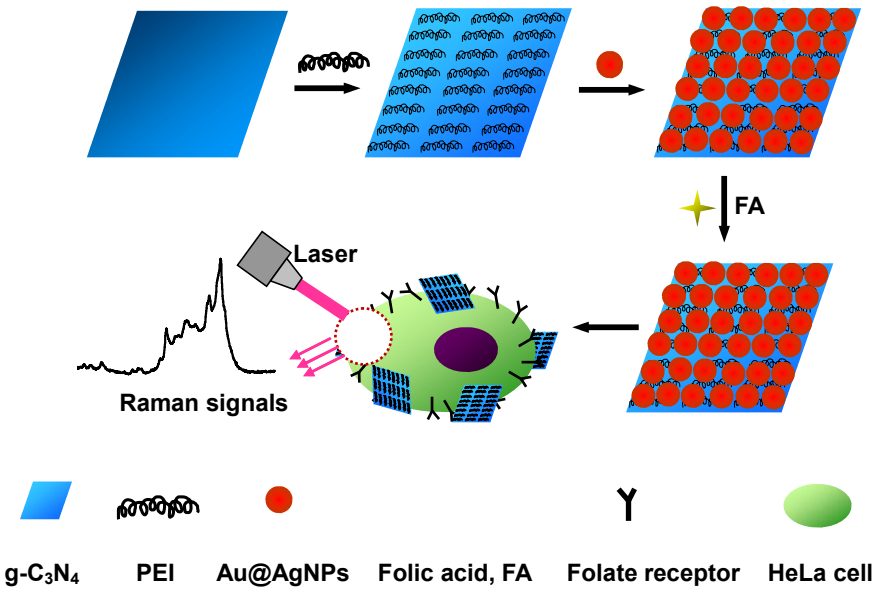

Fig. 1 The schematic illustration of the fabrication procedure of g-C_3N_4/Au@AgNPs-FA as SERS probe and its application in cancer cell diagnostics.

3. Results and discussion

The fabrication procedure of the g-C_3N_4/Au@AgNPs composite structure and its application in detection of cancer cells were shown in Fig.1. The Au@AgNPs were prepared by AuNPs with the size of 30 nm as the "seeds" and ascorbic acid solution as reductive agent, subsequently the silver nitrate solution was added drop by drop under vigorous stirring.[1b] Because the crystalline of Au and Ag match very well, the resultant Ag was selectively grown on the surface of the gold particles to form the core-shell Au@AgNPs (~45 nm in diameter), accompanying an obvious color change from wine red to orange (Fig.S1, ESI†).

Benefiting from the unique physical and chemical properties such as high surface area, remarkable biocompatibility and ease of functionalization, the 2D layered nanomaterials have shown great potentials in biochemistry and biomedicine.[19] The metal-free g-C_3N_4 was a typical 2D nanomaterials with good biocompatibility and low toxicity. The g-C_3N_4 bulk materials were obtained by the polymerization of melamine molecules (Fig.S2, ESI†). The ultrathin g-C_3N_4 nanosheets were obtained by sonicating bulk g-C_3N_4 in water for about 20 h (Fig.S3, ESI†). As could be seen from Fig.S4, the IR spectrum of g-C_3N_4 nanosheets showed nearly indentical absorption bands with bulk g-C_3N_4, and the Raman spectra of them were also almost the same (Fig.S5, ESI†). The above experimental results confirmed that the intrinsic properties of ultrathin g-C_3N_4 nanosheets had not changed compared with the bulk materials.

The zeta potential of the resulting ultrathin g-C_3N_4 nanosheets was about -35.8 mV, which indicated that they were negatively charged (Table S1, ESI†). On the other hand, the Au@AgNPs were also negatively charged, with the zeta potential of about -42.6 mV. Based on the electrostatic repulsion between the same charge, so the ultrathin g-C_3N_4 nanosheets were very weak for anchoring Au@AgNPs directly onto the them. In order to solve the above problems, the ultrathin g-C_3N_4 was first modified by polyvinylpyrrolidone (PVP). PVP is a nontoxic and biocompatible polymer surfactant, which is often used as a stabilizing agent and dispersing agent in the preparation of nanostructures.[20] Then a positively charged polymer named poly(ethyleneimine) (PEI) was used to modify the ultrathin g-C_3N_4 nanosheets. PEI is positively charged because there are so many basic amino on the the polymer chains.[1a] Finally, the PEI molecules which modified on the ultrathin g-C_3N_4 nanosheets can anchor the negatively charged nanoparticles onto the g-C_3N_4 nanosheets. At last, the FA was attached to the g-C_3N_4/Au@AgNPs via non-covalent binding. FA was used as not only Raman reporter molecule but also targeting molecule to distinguish the cancer cells.

The morphologies of ultrathin g-C_3N_4 nanosheets and Au@AgNPs-decorated ultrathin g-C_3N_4 nanosheets were characterized by transmission electron microscopy (TEM).

Fig.2A showed the typical TEM image of ultrathin g-C_3N_4 nanosheets. The water suspension of ultrathin g-C_3N_4 nanosheets was nearly transparent, and its concentration was estimated to be 0.15 mg/mL.[14] The dynamic light scattering data showed that the dimension of the ultrathin g-C_3N_4 nanosheets more than 100 nm, mainly in the 200 nm to 600 nm region (Fig.S6, ESI†). As shown in Fig. 2B-E, all of the Au@AgNPs which had uniform size and shape were confined in the range of ultrathin g-C_3N_4 nanosheets. The concentration of Au@AgNPs was about 0.20 nM based on the concentration of AuNPs seed (calculated using Beer's law and the extinction coefficient).[1b] In order to achieve the optimum SERS activity, the ultrathin g-C_3N_4 nanosheets loaded with Au@AgNPs were examined by changing the concentrations of Au@AgNPs and keep identical ultrathin g-C_3N_4 nanosheets (0.15 mg/mL). The concentration of Au@AgNPs was changed from 0.05 to 0.40 nM. Only few nanoparticles were dispersed on the ultrathin g-C_3N_4 nanosheets after 0.05 nM Au@AgNPs addition (Fig. 2B). When the concentration of Au@AgNPs was increasing, the nanoparticles loaded on the ultrathin g-C_3N_4 nanosheets became obviously intensive (Fig. 2C). As the concentration of Au@AgNPs was up to 0.20 nM, a uniform, high density Au@AgNPs decorated ultrathin g-C_3N_4 nanosheets nanocomposite was obtained (Fig. 2D). When the concentration of Au@AgNPs was increased to 0.40 nM, it was clearly observed most areas of the nanocomposite were dark color, which was mainly due to the overlapping of the loaded Au@AgNPs (Fig. 2E). The HRTEM images (Fig.S7, ESI†) and chemical maps of the g-C_3N_4/Au@AgNPs (Fig.S8, ESI†) were obtained, which further clearly showed the hybrid structure. The g-C_3N_4/Au@AgNPs nanocomposite was also confirmed by XRD, and the diffraction peaks and relative intensity matched with standard g-C_3N_4 and Au@AgNPs powder diffraction data. (Fig.S9, ESI†).

The Au@AgNPs loaded on the surface of ultrathin g-C_3N_4 nanosheets was also confirmed by the UV-vis spectra. As shown in Fig. 2F, when Au@AgNPs were loaded on the ultrathin g-C_3N_4 nanosheets, a new absorption peak corresponding to the Au@AgNPs plasmon with a wavelength of 350-550 nm emerged. The line of Fig. 2F from "a" to "e" corresponding to Fig. 2A-E, respectively. As the number of Au@AgNPs loaded on the ultrathin g-C_3N_4 nanosheets increased, the absorption peaks mentioned above were becoming more and more strong. Once mixed, a distinct color change was observed as the suspension changed from nearly transparent to orange with the concentration of Au@AgNPs increasing.

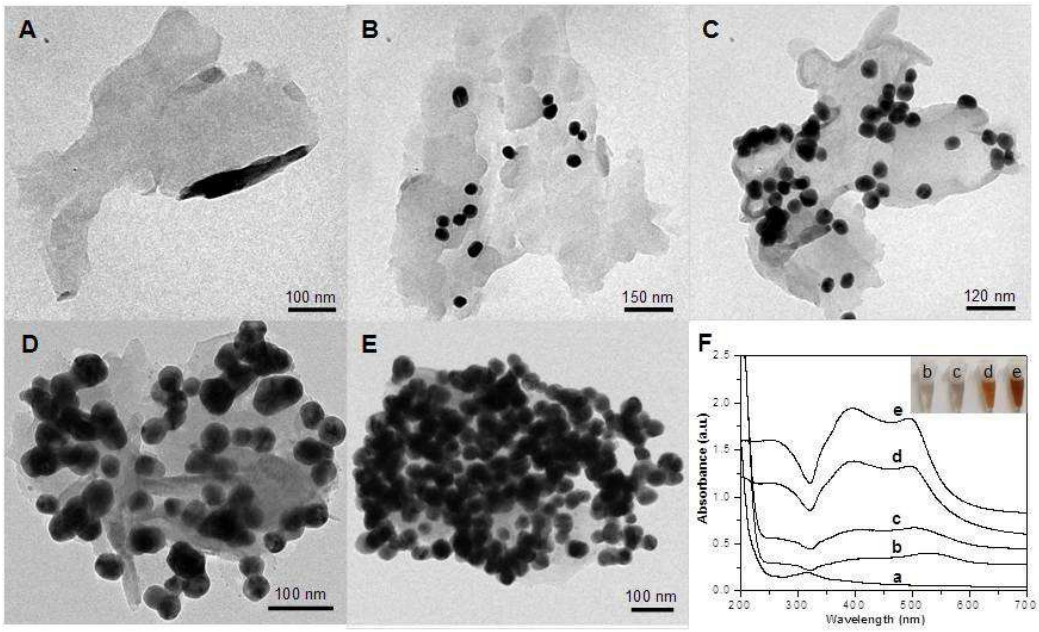

Fig. 2 TEM images of ultrathin g-C_3N_4 nanosheets (A) and the g-C_3N_4/Au@AgNPs nanocomposites with identical ultrathin g-C_3N_4 nanosheets (0.15 mg/mL) prepared with various concentrations Au@AgNPs: (B) 0.05 nM, (C) 0.10 nM, (D) 0.20 nM, (E) 0.40 nM. (F) The corresponding UV-vis absorption spectra of the samples shown in A-E. (inset: the corresponding photographs under daylight).

To further determine the layers of the g-C_3N_4 nanosheets, atomic force microscope (AFM) measurements were also obtained. As shown in Fig. 3A, the ultrathin g-C_3N_4 nanosheets nearly had the same thickness. At the same time, Fig. 3B showed the average height of the g-C_3N_4 nanosheets randomly measured was about 1.2 nm, which indicated that the ultrathin nanosheets were comprised of about three layer forms.[13-14] The AFM was also used to study the g-C_3N_4/Au@AgNPs nanocomposite in Fig. 2D. According to the AFM and height images, the changing of the thickness and roughness were monitored. As shown in Fig. 3C, the Au@AgNPs with the diameter around 45 nm were loaded on the surface of g-C_3N_4 nanosheets. After loading of the Au@AgNPs, it was observed that the roughness of the nanosheets increased and lots of nanoparticles were found. As shown in Fig. 3D, the thickness of the g-C_3N_4/Au@AgNPs hybrid was demonstrated from 50 to 90 nm which significantly thicker than the g-C_3N_4 nanosheets, indicating that the Au@Ag nanoparticles were assembled on the g-C_3N_4 corresponding to the TEM image. Finally, the AFM image showed the formation of nanocomposites and proved that the loading of Au@AgNPs was

efficient on the platform of g-C_3N_4 nanosheets.

In order to optimize the performance of the g-C_3N_4/Au@AgNPs hybrids as SERS substrate, the g-C_3N_4 nanosheets decorated with different amounts Au@AgNPs had been synthesized in Fig. 2B-E. To choose the best SERS active substrate, the same conventional Raman-active probe R6G (1.0×10^{-13} M) was used to evaluate the SERS activity of these hybrids with loading different density Au@AgNPs (Fig.S10, ESI†). The strong Raman peaks at 612 cm^{-1}, 774 cm^{-1}, 1360 cm^{-1}, 1509 cm^{-1} and 1650 cm^{-1} were in good agreement with the previous reports of pure R6G.[21] Weak Raman spectra of R6G were detected on the Au@AgNPs, while much stronger signals of R6G were obtained from g-C_3N_4/Au@AgNPs nanocomposites. Furthermore, the Raman signals of R6G were getting stronger with the increasement of the Au@AgNPs decorated on the ultrathin nanosheets. The "hot spots" were formed in the nanoscale gaps among the Au@AgNPs. At the same time, the arrangement of Au@AgNPs on the ultrathin g-C_3N_4 nanosheet were not very close, therefore, there were still many blanks between the Au@AgNPs for the enrichment of analyte molecules in the process of SERS detection. When the density of loaded Au@AgNPs further increased, however, particles overaggregate was bad to SERS signals and the stability of nanocomposites solution. In our experiments, the g-C_3N_4/Au@AgNPs nanocomposite in Fig. 2D had the best performances in SERS activity and was chosen for all the following tests.

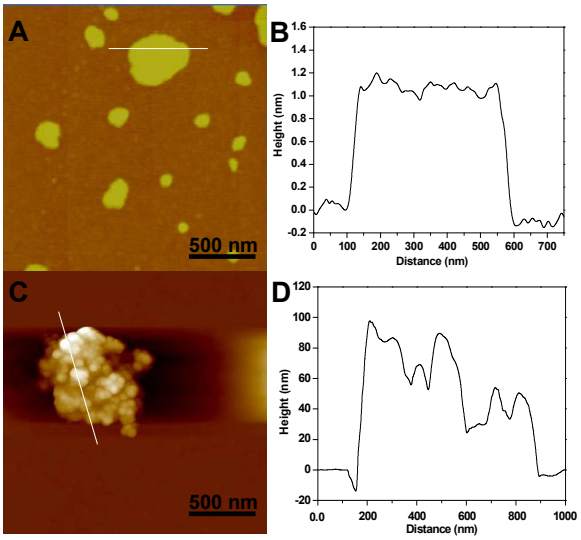

Fig. 3 AFM and correspondging height images of ultrathin g-C_3N_4 nanosheets (A, B) and g-C_3N_4/Au@AgNPs nanocomposites (C, D).

To study the SERS performance of g-C_3N_4/Au@AgNPs above mentioned, the SERS spectra of R6G with concentrations ranging from 1.0×10^{-9} to 1.0×10^{-17} M were obtained. As shown in Fig. 4A, the Raman signal were still be observed even the concentration of R6G decreased to as low as 1.0×10^{-17} M. The SERS intensity of R6G at 1360 cm^{-1} with different concentrations clearly showed g-C_3N_4/Au@AgNPs hybrids had excellent SERS activity (Fig.S11, ESI†). In addition, the uniformity of sensitivity of SERS substrate at every site was very important for SERS substrates. As shown in Fig.S12, the Raman spectra of R6G with concentration of 1.0×10^{-13} M were obtained from ten random sites, suggesting the good uniformity of g-C_3N_4/Au@AgNPs (Fig.S12, ESI†). The high SERS performance of g-C_3N_4/Au@AgNPs nanocomposite could be attributed to the huge surface of g-C_3N_4 nanosheets to adsorb more target molecules and the strong electromagnetic enhancement of the Au@Ag NPs. As shown in Fig. 4B, the SERS spectra of R6G (1.0×10^{-13} M) absorbed on the Au@AgNPs was also collected. The hybrids showed obviously stronger SERS signal than that of Au@AgNPs. The SERS experimentals confirmed that the ultrathin g-C_3N_4 nanosheets loaded Au@AgNPs nanocomposites had super sensitivity, high uniformity and excellent reproducibility as the substrate for Raman applications.

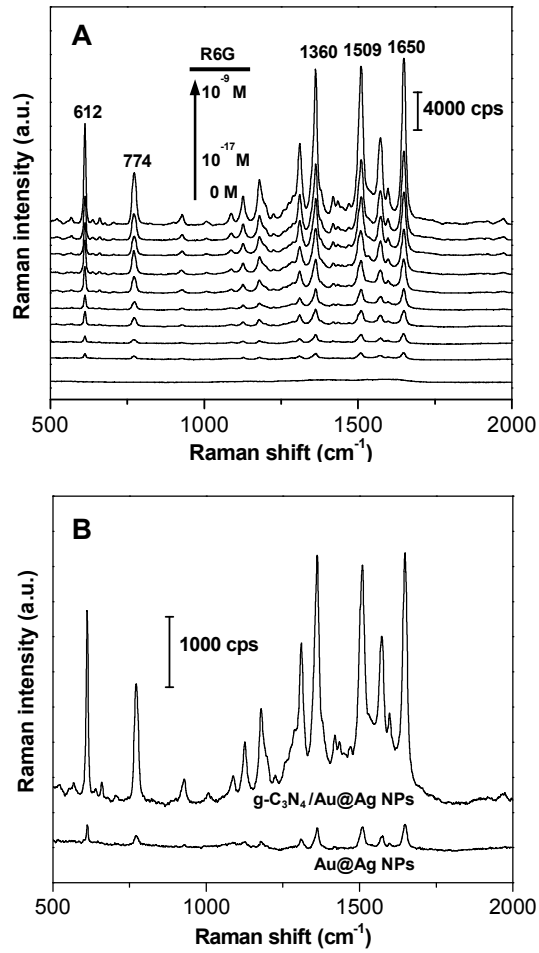

Fig. 4 The SERS activity of g-C_3N_4/Au@AgNPs. (A) SERS spectra of R6G molecules with the increase of R6G concentrations from 1.0×10^{-17} M to 1.0×10^{-9} M by a factor of 10 (the bottom line represents no added R6G), (B) SERS spectra of 1.0×10^{-13} M R6G molecules from g-C_3N_4/Au@AgNPs and Au@AgNPs, respectively.

The SERS spectra of FA with a series of concentrations were shown in Fig. 5. The Raman signal of FA were still be observed even the concentration decreased to as low as 10 nM. The main Raman peaks of FA were consistent with the previous work.[15] The intensity of the strongest peak at 1595 cm^{-1} was used for the quantitative evaluation of the FA level and exhibited a good linear relationship with the concentration ranging from 10 nM to 100 nM (R^2= 0.9976). The limit of detection was determined to be 2.41 nM was reached based on three standard deviations above the background. Therefore, the strong SERS signals of FA was

obtained from the g-C_3N_4/Au@AgNPs compared to Au@AgNPs , leading to the ultrasensitive detection of FA (Fig.S13, ESI†). In order to obtain a better understanding of hybrids, the g-C_3N_4 nanosheets/AgNPs (g-C_3N_4/AgNPs) nanocomposites was also prepared similarly. Taking R6G for example, the g-C_3N_4/Au@AgNPs exhibited an excellent Raman activity by 3 orders of magnitude higher than the corresponding g-C_3N_4/AgNPs (Fig.S14, ESI†). The g-C_3N_4/Au@AgNPs nanocomposites owning high SERS activity and stability of the water-soluble endowed them as a promising material for bioimaging application.

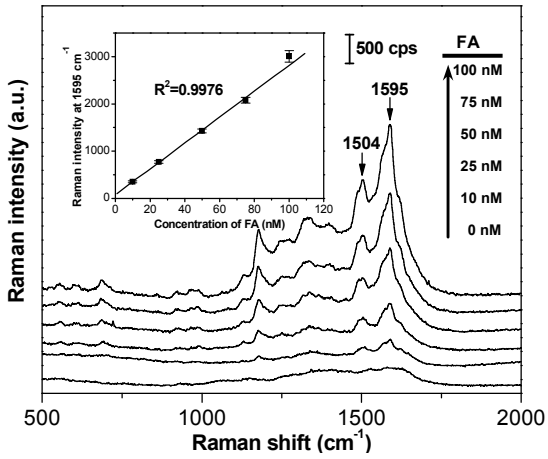

Fig. 5 SERS spectra of FA with different concentrations (0 nM, 10 nM, 25 nM, 50 nM, 75 nM and 100 nM) obtained from g-C_3N_4/Au@AgNPs. The inset was the linear correlation of Raman intensity (at 1595 cm^{-1}) with the FA concentrations from 10 nM to100 nM.

In this work, the FA was used as both the Raman probe molecule and the targeting ligand for cancer cells with FRs. FA was attached to the surface of g-C_3N_4/Au@AgNPs by physisorption, and the non-covalent interaction between them was attributed to π-π* stacking.[22] Based on the above content, the g-C_3N_4 nanosheets was used to enrich the FA molecules, at the same time the Au@AgNPs loaded on the nanosheets enhanced the Raman signal of FA. The Raman characteristic signals of FA could be used to identify FA on certain cancer cells by using g-C_3N_4/Au@AgNPs-FA as diagnostic probe materials.

The modification of FA with g-C_3N_4/Au@AgNPs through physisorption was confirmed by the new absorption peaks at 280 and 365 nm corresponding to the standard FA (Fig.S15, ESI†). The cytotoxicity of g-C_3N_4/Au@AgNPs-FA was investigated using MTT assay which had been described as a suiable method for the detection of nanoparticle toxicity. As can be seen from the Fig.S16, very little loss of cell viability was observed even with the concentration of incubated g-C_3N_4/Au@AgNPs-FA as high as 300 μg/mL, suggesting the excellent biocompatibility and nontoxicity of the hybrids. In addition, it was worth mentioning that the concentration of g-C_3N_4/Au@AgNPs-FA used in bioimaging experiment was much lower only 150 μg/mL.

To investigate the targeting ability of the g-C_3N_4/Au@AgNPs-FA, the Hela cells were used as model cancer cells because they over-express the FRs (FRs-positive), and A549 cells were selected as control which express few FRs (FRs-negative). The HeLa and A549 cells cultured in Dulbecco's modified Eagle's medium (DMEM) were incubated with g-C_3N_4/Au@AgNPs-FA for 2 h and washed sufficiently with phosphate-buffered saline (PBS) before experiments. The dark-field images indicated that a large number of the g-C_3N_4/Au@AgNPs-FA nanocomposites had been attached to the FRs after 2 h incubation (Fig. 6A and C). However, only a small amount of nanocomposites had been attached on A549 cells, indicating the specific targeting of g-C_3N_4/Au@AgNPs-FA to FRs-positive cancer cells. The SERS imagings of HeLa and A549 cells with FA at 1595 cm^{-1} shown in Fig. 6C and D, which clearly displayed that the SERS signals almost appeared on the surface of cells. The results also showed that HeLa cells exhibited significant Raman signals of FA and thus more distingguishable Raman image was received. The Fig. 6E and F described the corresponding Raman at the indicated sites. It was clear that the SERS spectra of FA observed and not overwhelmed by the large background, but the signals of FA were too weak to be distinguished after incubated with FRs-negatived A549 cells. The above experimentals clearly demonstrated that our SERS probe was able to distingguish FRs over-expressed cancer cells from the cells that expressed few FRs.

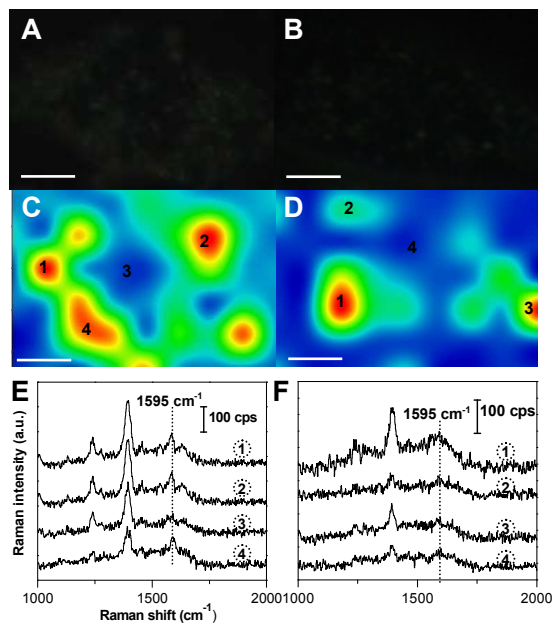

Fig. 6 Dark-field images and corresponding SERS images from the peak of FA at 1595 cm^{-1} with HeLa cells (A,C) and A549 cells (B, D) after incubated with g-C_3N_4/Au@AgNPs-FA. (E) and (F) showed the Raman spetra of the spots marked in (C) and (D), respectively. Scale bars = 5 μm.

4 CONCLUSIONS

In conclusion, we reported the synthesis of a functional g-C_3N_4/Au@AgNPs-FA hybrid material with good biocompatibility and targeting ability, and its application in Raman diagnosis of cancer cells. The obtained g-C_3N_4/Au@AgNPs showed tremendous enhancement in the Raman signals of the absorbed FA, which has the ability in targeting FRs-positive cancer cells and used as Raman reporter. The SERS signals of the FA molecules on the FRs-positive cancer cells were successfully detected with 532 nm laser excitation. The aboved experimental results indicate that the g-C_3N_4/Au@AgNPs-FA has not only

good targeting capability with live cancer cells but also great potential as a new Raman probe for cancer diagnosis.

Acknowledgements

This work was supported by the National Science Foundation of China (Nos. 21371174, 21175137, 21375131, 61205152).

Notes and references

[a] *Institute of Intelligent Machines, Chinese Academy of Sciences, Hefei, Anhui, 230031, China. E-mail: cljiang@iim.ac.cn; zpzhang@iim.ac.cn*
[b] *Department of Chemistry, University of Science & Technology of China, Hefei, Anhui, 230026, China.*
[c] *State Key Laboratory of Transducer Technology Chinese Academy of Sciences, Hefei, Anhui, 230031, China.*
† Electronic Supplementary Information (ESI) available: [details of any supplementary information available should be included here]. See DOI: 10.1039/b000000x/.

1 (a) L. L. Zhang, C. L. Jiang and Z. P. Zhang, *Nanoscale*, 2013, **5**, 3773-3779; (b) B. H. Liu, G. M. Han, Z. P. Zhang, R. Y. Liu, C. L. Jiang, S. H. Wang and M. Y. Han, *Anal. Chem.,* 2012, **84**, 255-261.
2 (a) J. P. Wang, L. Yang, B. H. Liu, H. H. Jiang, R. Y. Liu, J. W. Yang, G. M. Han, Q. S. Mei and Z. P. Zhang, *Anal. Chem.,* 2014, 8**6**, 3338-3345; (b) H. Ko and V. V. Tsukruk, *Small,* 2008, **4**, 1980-1984.
3 S. J. Lee and M. Moskovits, *Nano Lett.,* 2011, **11**, 145-150.
4 (a) Z. X. Chen, J. J. Li, X. Q. Chen, J. T. Cao, J. R. Zhang, Q. H. Min and J. J. Zhu, *J. Am. Chem. Soc.,* 2015, **137**, 1903-1908; (b) S. R. Panikkanvalappil, S. M. Hira, M. A. Mahmoud and M. A. El-Sayed, *J. Am. Chem. Soc.,* 2014, **136**, 15961-15968.
5 (a) C. L. Zavaleta, B. R. Smith, I. Walton, W. Doering, G. Davis, B. Shojaei, M. J. Natan and S. S. Gambhir, *Proc. Natl. Acad. Sci. U. S. A.* 2009, **106**, 13511-13516; (b) V. Amendola, S. Scaramuzza, L. Litti, M. Meneghetti, G. Zuccolotto, A. Rosato, E. Nicolato, P. Marzola, G. Fracasso, C. Anselmi, M. Pinto and M. Colombatti, *Small,* 2014, **10**, 3823-3823; (c) J. Huang, C. Zong, H. Shen, M. Liu, B. A. Chen, B. Ren and Z. J. Zhang, *Small,* 2012, **8**, 2577-2584.
6 (a) S. Schlucker, *Angew. Chem., Int. Ed.,* 2014, **53**, 4756-4795; (b) W. E. Smith, *Chem. Soc. Rev.,* 2008, **37**, 955-964.
7 (a) K. Kneipp, Y. Wang, H. Kneipp, L. T. Perelman, I. Itzkan, R. Dasari and M. S. Feld, *Phys. Rev. Lett.,* 1997, **78**, 1667-1670; (b) S. M. Nie and S. R. Emery, *Science* 1997, **275**, 1102-1106.
8 (a) Z. Y. Wang, S. F. Zong, W. Li, C. L. Wang, S. H. Xu, H. Chen and Y. P. Cui, *J. Am. Chem. Soc.,* 2012, **134**, 2993-3000; (b) T. X. Yang, X. Y. Guo, H. Wang, S. Y. Fu, J. Yu, Y. Wen and H. F. Yang, *Small,* 2014, **10**, 1325-1331; (c) Z. L. Song, Z. Chen, X. Bian, L. Y. Zhou, D. Ding, H. Liang, Y. X. Zou, S. S. Wang, L. Chen, C. Yang, X. B. Zhang and W. H. Tan, *J. Am. Chem. Soc.,* 2014, **136,** 13558-13561.
9 (a) K. S. Novoselov, D. Jiang, F. Schedin, T. J. Booth, V. V. Khotkevich, S. V. Morozov and A. K. Geim, *Proc. Natl. Acad. Sci. U. S. A.* 2005, **102**, 10451-10453; (b) K. P. Loh, Q. L. Bao, G. Eda and M. Chhowalla, *Nat. Chem.,* 2010, **2**, 1015-1024; (c) J. Q. Tian, Q. Liu, A. M. Asiri, K. A. Alamry and X. P. Sun, *Chem. Sus. Chem.*, 2014, **7**, 2125-2130; (d) N. Y. Cheng, J. Q. Tian, Q. Liu, C. J. Ge, A. H. Qusti, A. M. Asiri, A. O. Al-Youbi and X. P. Sun, *ACS Appl. Mater. Interfaces,* 2013, **5**, 6815-6819.
10 Y. Wang, X. C. Wang and M. Antonietti, *Angew. Chem., Int. Ed.,* 2012, **51**, 68-89.
11 (a) C. M. Cheng, Y. Huang, X. Q. Tian, B. Z. Zheng, Y. Li, H. Y. Yuan, D. Xiao, S. P. Xie and M. M. F. Choi, *Anal. Chem.,* 2012, **84**, 4754-4759; (b) N. Y. Cheng, P. Jiang, Q. Liu, J. Q. Tian, A. M. Asiri and X. P. Sun, *Analyst,* 2014, **139**, 5065-5068; (c) J. Q. Tian, Q. Liu, A. M. Asiri, A. O. Al-Youbi and X. P. Sun, *Anal. Chem.,* 2013, **85**, 5595-5599.
12 (a) X. R. Du, G. J. Zou, Z. H. Wang and X. L. Wang, *Nanoscale,* 2015, **7**, 8701-8706; (b) J. Q. Tian, Q. Liu, A. M. Asiri, A. H. Qusti, A. O. Al-Youbi and X. P. Sun, *Nanoscale*, 2013, **5**, 11604-11609; (c) J. Q. Tian, Q. Liu, C. J. Ge, Z. C. Xing, A. M. Asiri, A. O. Al-Youbi and X. P. Sun, *Nanoscale*, 2013, **5**, 8921-8924.
13 L. S. Lin, Z. X. Cong, J. Li, K. M. Ke, S. S. Guo, H. H. Yang and G. N. Chen, *J. Mater. Chem. B,* 2014, **2**, 1031-1037.
14 X. D. Zhang, X. Xie, H. Wang, J. J. Zhang, B. C. Pan and Y. Xie, *J. Am. Chem. Soc.,* 2013, **135**, 18-21.
15 W. Ren, Y. X. Fang and E. K. Wang, *Acs Nano,* 2011, **5**, 6425-6433.
16 (a) H. F. Dong, J. P. Lei, H. X. Ju, F. Zhi, H. Wang, W. J. Guo, Z. Zhu and F. Yan, *Angew. Chem., Int. Ed.,* 2012, **51**, 4607-4612; (b) D. Feng, Y. C. Song, W. Shi, X. H. Li and H. M. Ma, *Anal. Chem.,* 2013, **85**, 6530-6535.
17 D. J. Bharali, D. W. Lucey, H. Jayakumar, H. E. Pudavar and P. N. Prasad, *J. Am. Chem. Soc.,* 2005, **127**, 11364-11371.
18 (a) J. J. Castillo, T. Rindzevicius, L. V. Novoa, W. E. Svendsen, N. Rozlosnik, A. Boisen, P. Escobar, F. Martinez and J. Castillo-Leon, *J. Mater. Chem. B,* 2013, **1**, 1475-1481; (b) C. F. Hu, Y. L. Liu, J. L. Qin, G. T. Nie, B. F. Lei, Y. Xiao, M. T. Zheng and J. H. Rong, *ACS Appl. Mater. Interfaces,* 2013, **5**, 4760-4768.
19 G. H. Yang, C. Z. Zhu, D. Du, J. J. Zhu and Y. H. Lin, *Nanoscale,* 2015, DOI: 10.1039/C5NR03398E.
20 (a) X. C. Qin, Z. Y. Guo, Z. M. Liu, W. Zhang, M. M. Wan and B. W. Yang, *J. Photoch. Photobio. B.,* 2013, **120**, 156-162; (b) A. S. Wajid, S. Das, F. Irin, H. S. T. Ahmed, J. L. Shelburne, D. Parviz, R. J. Fullerton, A. F. Jankowski, R. C. Hedden and M. J. Green, *Carbon,* 2012, **50**, 2065-2065.
21 G. F. Li, H. Li, Y. J. Mo, X. J. Huang and L. Q. Chen, *Chem. Phys. Lett.,* 2000, **330**, 249-254.
22 M. C. Rong, L. P. Lin, X. H. Song, T. T. Zhao, Y. X. Zhong, J. W. Yan, Y. R. Wang and X. Chen, *Anal. Chem.,* 2015, **87**, 1288-1296.